ACS APPLIED MATERIALS & INTERFACES

Research Article

www.acsami.org

Electrospun Nanofibrous P(DLLA–CL) Balloons as Calcium Phosphate Cement Filled Containers for Bone Repair: in Vitro and in Vivo Studies

Xunwei Liu,[†,§] Daixu Wei,[‡,§] Jian Zhong,[*,‡] Mengjia Ma,[⊥] Juan Zhou,[‡] Xiangtao Peng,[†] Yong Ye,[†] Gang Sun,[*,†] and Dannong He[*,‡,⊥]

[†]Department of Medical Imaging, Jinan Military General Hospital, No. 25 Shifan Road, Jinan 200050, Shandong Province, People's Republic of China

[‡]National Engineering Research Center for Nanotechnology, No. 28 East Jiangchuang Road, Minhang District, Shanghai 200241, People's Republic of China

[⊥]School of Materials Science and Engineering, Shanghai Jiao Tong University, No. 800 Dongchuang Road, Minhang District, Shanghai 200240, People's Republic of China

Supporting Information

ABSTRACT: The spinal surgeon community has expressed significant interest in applying calcium phosphate cement (CPC) for the treatment of vertebral compression fractures (VCFs) and minimizing its disadvantages, such as its water-induced collapsibility and poor mechanical properties, limiting its clinical use. In this work, novel biodegradable electrospun nanofibrous poly(D,L-lactic acid–ϵ-caprolactone) balloons (ENPBs) were prepared, and the separation, pressure, degradation, and new bone formation behaviors of the ENPBs when used as CPC-filled containers in vitro and in vivo were systematically analyzed and compared. CPC could be separated from surrounding bone tissues by ENPBs in vitro and in vivo. ENPB-CPCs (ENPBs serving as CPC-filled containers) exerted pressure on the surrounding bone microenvironment, which was enough to crush trabecular bone. Compared with the CPC implantation, ENPB-CPCs delayed the degradation of CPC (i.e., its water-induced collapsilibity). Finally, possible mechanisms behind the in vivo effects caused by ENPB-CPCs implanted into rabbit thighbones and pig vertebrae were proposed. This work suggests that ENPBs can be potentially applied as CPC-filled containers in vivo and provides an experimental basis for the clinical application of ENPBs for the treatment of VCFs. In addition, this work will be of benefit to the development of polymer-based medical implants in the future.

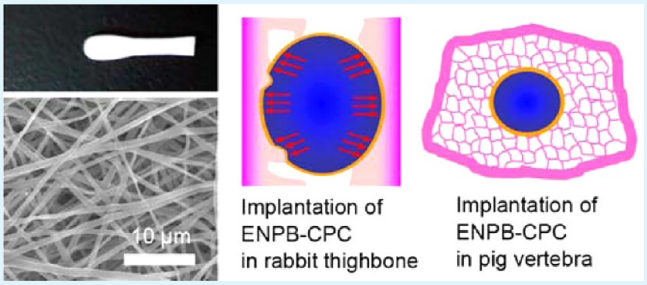

KEYWORDS: *calcium phosphate cement, electrospun nanofibrous P(DLLA-CL) balloons, in vitro, in vivo, pig vertebra, rabbit thighbone*

1. INTRODUCTION

It is a known fact that the incidence of vertebral compression fractures (VCFs) is increasing worldwide. VCFs are generally common in patients with osteoporosis, multiple myeloma, and trauma.[1] Since 1992, approximately 24% of women older than 50 years of age and 40% of women older than 80 years of age have experienced VCFs.[2] Additionally, most patients with VCFs have to endure sleep loss, decreased mobility, chronic pain, and significant limitations on the performance of everyday tasks.[2,3] Currently, traditional conservative treatment, traditional surgical treatment, and minimally invasive treatment are employed in clinics for the treatment of VCFs.[4−10] Because of the advantages of smaller incisions, shorter treatment times, reduced pain, and shorter recovery times, minimally invasive treatment has been increasingly used and accepted by surgeons and patients.

For minimally invasive clinical treatments, poly(methyl methacrylate) (PMMA) cement has typically been applied as a vertebral cement material in recent decades because of its appropriate fluidity, inertness, and good biomechanical properties.[11,12] However, its limitations of use include the potential toxicity of its monomers, its high polymerization temperature, its lack of direct bone apposition, and no sacralization cannot be ignored.[13−15] Therefore, calcium phosphate cement (CPC) has been explored by spinal surgeons as a substitute for the treatment of VCFs.[12] CPC has a specific elementary composition and a microporous structure that closely resembles natural bone and offers many advantages in comparison to

Received: June 3, 2015
Accepted: August 10, 2015
Published: August 10, 2015

DOI: 10.1021/acsami.5b04868
ACS Appl. Mater. Interfaces 2015, 7, 18540−18552

PMMA cement, such as the induction of biological degradation and bone formation for the replacement of defects with new bone, as well as the capacity to restore the mass and height of the fractured vertebral body.[12,16,17]

The water-induced collapsibility and poor mechanical properties of CPC might induce subsequent augmentation failure during VCF tratment[18] and therefore limit the application of CPC in the clinical treatment of VCFs. CPC is rapidly degraded and leaked into water, which is called water-induced collapsibility. The compressive strength of CPC is less than that of the natural bone cortex. Moreover, the rapid collapsibility of CPC decreases its mechanical properties. The poor mechanical properties of CPC may limit the use of CPC in applications designed to support spinal alignment.[12] Many reports have indicated that CPC leakage outside a fractured vertebral body might induce common complications such as pulmonary embolism, nerve damage, and even death.[19,20] To the best of our knowledge, thus far only a Vessel-X filling container (A-Spine Asia Co., Ltd., Taiwan, China)[21] and an expandable metallic stent[22] have been designed to decrease the leakage of PMMA bone cement. However, these devices have mesh sizes of 100-μm and millimeter levels, respectively. Therefore, they cannot prevent the water-induced collapsibility of CPC. To improve the mechanical properties of CPC, the incorporation of high-strength biomaterials into CPC has been widely explored. The incorporation of chitosan lactate[23] and collagen[24] into CPC was explored as a method of increasing its mechanical properties. The addition of electrospun poly(lactic acid) and poly(lactic-*co*-glycolic acid) fibers maintained the mechanical properties of CPC−gelatin cements for longer periods of time.[25] However, the mechanical properties of the incorporated CPC were still not sufficient to ensure CPC application in load-bearing bones. This is largely due to the poor structural interface that exists between the hydrophobic polymer and the hydrophilic mineral.

To minimize the water-induced collapsibility of CPC and increase its mechanical properties, we recently developed novel biodegradable electrospun nanofibrous poly(D,L-lactic acid−ϵ-caprolactone) [P(DLLA−CL)] balloons (ENPBs) using an electrospinning technique.[26] P(DLLA−CL) is composed of a biodegradable copolymer of D,L-lactic acid and ϵ-caprolactone. The purpose of using ENPBs as CPC-filled containers is not to address the poor structural interface that exists between the hydrophobic polymer and the hydrophilic mineral but rather to exploit the increase in the amount of pressure applied to CPC by inhibiting the disordered flow of CPC in the presence of an encapsulating balloon prior to its solidification. Electrospun nanofibrous P(DLLA−CL) scaffolds had a good tensile ability. ENPBs can be inflated if CPC is injected into it. Therefore, an ENPB can be designed as a CPC container to restore the height of a fractured vertebral body. Our previous in vitro results initially showed that the ENPBs could separate the CPCs from surrounding bone tissues and that they could degrade in degradation solutions. Moreover, in vitro results have shown that the ENPB-CPC (ENPB as the CPC filling container) has sufficient load-bearing ability to restore the height of a fractured vertebral body. However, although systematic comparisons between the in vitro and in vivo behaviors of ENPBs are important before they are evaluated in the clinic, such comparisons were not made in our previous work.

Polymer materials have been widely used as biomedical materials.[27−31] Many synthetic polymer biomaterials similar to P(DLLA−CL), such as PDLLA,[32−35] PLGA,[36,37] P(LLA−CL),[38] and PCL,[39,40] have been assessed in vivo to determine their behaviors in the bone microenvironments of sheep,[32,33,35,36] rabbit,[34,37] and pig.[38−40] However, there have been no reports evaluating the in vivo behaviors of P(DLLA−CL) biomaterials in bone microenvironments thus far. Therefore, an in vivo evaluation of ENPB scaffolds in bone microenvironments will not only validate the potential clinical application of using ENPBs as CPC-filled containers but also benefit the development of a P(DLLA−CL)-based medical implant in the future.

2. MATERIALS AND METHODS

2.1. Materials. All of the general chemicals that were used in this work were of analytical grade and were bought from Sinopharm Chemical Reagent Co., Ltd. (Shanghai, China). The block copolymer of P(DLLA−CL) (70:30) was bought from Jinan Daigang Biomaterial Co., Ltd. (Shandong, China) and had an inherent viscosity of 2.3 dL/g. Commercial CPC was bought from Shanghai Rebone Biomaterials Co., Ltd. (Shanghai, China). Commercial CPC has a powder component (calcium phosphate salts) and a curing liquid component. CPC was sterilized with epoxy ethane and packaged by the company. According to the instructions included with the commercial CPC, the setting time is 3−20 min and the compressive strength of the fully solidified CPC is approximately 35 MPa. Simulated body fluid was prepared according to previous works, using the following solution:[41,42] 50 mM Tris base, 137 mM NaCl, 4 mM $NaHCO_3$, 3 mM KCl, 1 mM K_2HPO_4, 1.5 mM $MgCl_2$, 2.5 mM $CaCl_2$, and 0.5 mM Na_2SO_4, pH 7.4. Lipase from pig pancreas and proteinase K from *Tritirachium album Limber* were purchased from Jianglai Biotech Co., Ltd. (Shanghai, China) and Merck (Mannheim, Germany), respectively, and then dissolved in 10 mM phosphate-buffered saline (PBS). Fresh human serum was obtained from the Department of Clinical Laboratory, Jinan Military General Hospital (Jinan, Shangdong, China).

2.2. P(DLLA−CL) Nanofiber and ENPB Fabrication. P(DLLA−CL) was dissolved in a dichloromethane−dimethylformamide (7:3, v/v) solution at a concentration of 6 wt % at 30 °C. Using a custom-designed electrospinning instrument, P(DLLA−CL) nanofibers were prepared and collected on a rotating titanium alloy mold to prepare the ENPBs (Figure 1A) according to our previous work.[26] Briefly, a 10 mL glass syringe filled with P(DLLA−CL) solution was fitted with a needle and placed on a KDS-200 syringe pump (Stoelting Co., Wood Dale, IL). The tip diameter of the needle was 0.9 mm. An applied voltage of 9−13 kV was produced using a high-voltage power supply (Teslaman HVPS Co., Ltd., Dalian, Liaoning, China). The feeding rate was approximately 0.3 mL/h. The rotating speed of the titanium alloy molds was 10−20 rpm. The collecting distance between the titanium alloy mold and the needle tip was approximately 10−15 cm. The ENPBs with a thickness of 0.15−0.20 mm were chosen for further research. The prepared ENPBs were dried under vacuum for 12 h and then stored in 1.5 mL centrifuge tubes at room temperature. The stocked ENPBs were soaked in medical-grade sterile water for 30 min prior to further in vitro study. The stocked ENPBs were packaged in a hermetically sealed container and sterilized by Co-60 γ irradiation for in vivo study.

2.3. In Vitro Simulated Degradation Experiments. Five types of degradation solutions were used to study the in vitro degradation behaviors of ENPBs: simulated body fluid (SBF), a 100 U/L lipase solution, a 3000 U/L lipase solution, a 20 mg/mL proteinase K solution, and fresh human serum. All of these solutions were filter-sterilized using 0.2 μm filters.

The ENPBs were cut into round ENPB scaffold patches weighing approximately 15 mg each. The cut ENPB scaffold patches were placed in a 50 mL test tube containing 20 mL of the degradation solution and incubated on a shake at 100 rpm at 37 °C for 42 days. The incubated degradation solutions were changed once weekly. At the designated time points, the ENPB scaffolds were taken out, washed three times with 40 mL of ultrapure water, and then dried under vacuum for 12 h.

DOI: 10.1021/acsami.5b04868
ACS Appl. Mater. Interfaces 2015, 7, 18540−18552

After these dried ENPB scaffold patches were weighed, their degradation rates (DRs) could be calculated according to eq 1.

$$\mathrm{DR}\ (\%) = [(W_a - W_b)/W_a] \times 100\% \quad (1)$$

where W_a and W_b are the weights of the dried ENPB scaffold patches before and after degradation, respectively. Morphological changes of the ENPB scaffold patches during the overall degradation process were visualized by scanning electron microscopy (SEM; Hitachi S-4800, Tokyo, Japan) at an accelerated voltage of 10 kV.

To measure the changes in the tensile properties of the material at different degradation times, ENPBs were formed on a round titanium alloy stick with a diameter of 10 mm. Then, the ENPBs were taken out and longitudinally cut into halves. Each half was cut into a test specimen with a length of 150 mm, a width of 10 mm, and a thickness of approximately 1 mm. The cut ENPB scaffold specimens were incubated in fresh human serum on a shake at 100 rpm at 37 °C. The incubated degradation solutions were changed once weekly. At the designated time points, ENPB specimens were taken out, washed three times, and then dried under vacuum for 12 h. Their tensile properties were measured using a universal testing machine (HY0230, Shanghai Hengyi Testing Instruments Co., Ltd., Shanghai, China) according to ISO 527-3:1995. The initial distance between grips was 100 mm, and the gauge length was 25 mm. The strain rate was 100 mm/mm. The tests were performed at room temperature (25 °C) and about 55% relative humility. Three parallel test specimens were investigated in this study.

2.4. Cell Culture on ENPB Scaffold Patches. Three types of cell lines were employed to study the in vitro cell biocompatibility of ENPB scaffold patches: mouse osteoblasts (MC 3T3-E1), human osteosarcoma cells (MG-63), and mouse embryonic fibroblasts (NIH 3T3). The cell lines were purchased from the Chinese Academy of Sciences (Shanghai, China). All of the cells were cultured in a cell culture medium in an incubator at 37 °C under a humidified 5.0% CO_2 atmosphere. The MC 3T3-E1 cells were cultured in MEM-α (Gibco, Carlsbad CA) with 10% fetal bovine serum (FBS; Gibco, Carlsbad, USA). The MG-63 and NIH 3T3 cells were cultured in Dulbecco's modified Eagle's medium (Gibco, Carlsbad, CA).

To prevent the cells from adhering onto the surfaces of 48-well tissue culture plates (TCPs), the TCPs were coated with 1.2% agarose. The ENPB scaffold patches were sterilized using a 75% (v/v) ethanol solution and then washed three times with 10 mM PBS. The ENPB scaffold patches were placed on the TCPs with agarose and pressed down using a hollow cylinder to prevent them from floating. The cells were cultured for 1, 4, and 7 days.

2.5. Confocal Laser Scanning Microscopy (CLSM) Observation of Cell Proliferation on ENPB Scaffold Patches. The distribution patterns of the three cell lines on the ENPBs were observed by CLSM (Leica, TCS SP5, Mannheim, Germany). Briefly, the cells on the ENPB scaffold patches were fixed in PBS with 4% paraformaldehyde for 20 min. Then, they were washed three times with PBS and immersed in PBS containing 0.5% Triton X-100 for 20 min. After permeabilization, the cells on the ENPB scaffold patches were washed three times with PBS and incubated in PBS with 5% FBS to block any nonspecific binding sites. Sequentially, they were incubated with Alexa Fluor 594 phalloidin (Life Tech, Grand Island, NY) for 30 min and 4′,6-diamidino-2-phenylindole (DAPI; Life Tech, Grand Island, NY) for 5 min at room temperature to stain the actins and cell nuclei, respectively. Finally, the distribution patterns of the staining in the cells on the ENPB scaffold patches were observed by CLSM.

2.6. SEM Observation of Cell Proliferation on ENPB Scaffold Patches. Morphological studies of in vitro cultured cells on the ENPB scaffold patches were performed using SEM (Hitachi S-4800, Tokyo, Japan). Briefly, the cells on the ENPB scaffold patches were washed three times with PBS to remove the culture medium and any unattached cells. Then, the cells were fixed in PBS with 5% glutaraldehyde for 12 h. The cells on the ENPB scaffold patches were dehydrated in an ethanol−water solution at a series of concentrations for 15 min, including concentrations of 30%, 50%, 70%, 90%, and 100% (v/v). Subsequently, the cells on the ENPB scaffold patches were dried under vacuum for 4 h to remove residual ethanol. Finally, the morphology of each cell type on the ENPB scaffold patches was observed by SEM at an accelerated voltage of 10 kV.

2.7. CCK-8 Assay of Cell Proliferation on ENPB Scaffold Patches. The cell viability on the ENPB scaffold patches was assessed using a cell counting kit-8 (CCK-8 Kit, Boya Biotech, Beijing, China).[43] Briefly, the culture medium was removed, and 450 μL of a medium containing 10% FBS and 50 μL of a CCK-8 solution was added into each well. The patches were incubated at 37 °C for 2 h, and 100 μL aliquots of supernatant were transferred into a 96-well plate. The absorbance was measured at 450 nm using an Infinite F50 microplate reader (TECAN, Switzerland). The absorbance was corrected by subtracting the absorbance of a mixture of 90 μL of a medium containing 10% FBS and 10 μL of CCK-8. For each group, six parallel experimental samples were used to assess the cell viability in this study.

2.8. Implantation of CPC or ENPB-CPC into Rabbit Thighbones. In this work, healthy New Zealand white rabbits with an age of 4 months and a weight of 2−2.5 kg were employed as animal models. A total of 48 rabbits (from the Animal Center in Jinan Military General Hospital) were randomly divided into two groups: (a) an ENPB-CPC group and (b) a CPC implantation group, which served as a control. CPC collapsibility occurred in 3 rabbits in the CPC group during surgery, which resulted in the death of the rabbits. Therefore, another 3 rabbits were added to the CPC group. The use of the rabbits and the experimental procedures in this study were approved by the Jinan Military General Hospital's Animal Care and Use Committee [No. SCXK(Lu)2010-0005].

The rabbits were anaesthetized, and the areas to be used for the surgeries were disinfected. Then, the biomaterials were implanted into the left thighbone of the animals (Figure 4A) by a minimally invasive surgical technique, which was monitored by digital subtraction angiography (DSA, GE, INNOVA 4100, USA). The ENPB-CPC implantation process was performed as follows. The rabbit thighbone was punctured via a skin incision trocar with a diameter of 4.0 mm (Figure 4B,C). The trocar needle was withdrawn and a bone drill was placed in to drill a circular hole as a working channel (Figure 4D). The bone drill was then withdrawn. The ENPBs were tied onto a balloon delivery tube and then delivered into the rabbit thighbone via the working channel (Figure 4E). CPC was prepared by mixing a liquid component and a powder component until a paste with a high viscosity was formed. The cement was loaded into a bone cement perfusion apparatus. Then, CPC was injected into the ENPBs using a pump. The inflation of the ENPB-CPCs was monitored by digital subtraction angiography (DSA; Figure 4F−I,J−M). Finally, the end of each ENPB-CPC was sealed by slow rotation of the balloon delivery tube. After that, the instruments were withdrawn. No CPC leakage outside of the ENPB was observed by DSA. The CPC implantation process was similar to that of the ENPB-CPC.

2.9. Implantation of CPC or ENPB-CPC into Pig Vertebrae. In this work, pigs with an age of 4 months and a weight of 80−100 kg were employed as an animal model. A total of 6 pigs were obtained from the Animal Center in Jinan Military General Hospital and the L2−L5 vertebrae of every pig were randomly divided into two groups: (a) an ENPB-CPC group and (b) a CPC implantation group, which served as a control. The use of the pigs and the experimental procedures in this study were approved by the Jinan Military General Hospital's Animal Care and Use Committee [No. SCXK(Lu)2010-0005].

The animals were anaesthetized, and the surgery sites were disinfected. Minimally invasive surgery was performed and monitored by DSA (GE, INNOVA 4100, USA). A postimplantation surgical site is shown in Figure 6A. The surgical process occurred as follows. The pig vertebrae were punctured using a skin incision trocar with an outer diameter of 4.0 mm (Figure 6B). The trocar needle was withdrawn and a bone drill was placed in to drill a circular hole with a diameter of 4.0 mm as a working channel (Figure 6C). For the CPC group, the bone drill was withdrawn, and CPC was directly injected into the vertebra, after which the instruments were withdrawn, and dispersed

DOI: 10.1021/acsami.5b04868
ACS Appl. Mater. Interfaces 2015, 7, 18540−18552

throughout the vertebra, as shown in a representative L4 vertebra in Figure 6D,E. For the ENPB-CPC group, the bone drill was withdrawn, and the ENPBs were tied onto a balloon delivery tube and then delivered into the vertebra via the working channel. Following this, CPC was injected into the ENPBs using a pump, as shown in a representative L5 vertebra in Figure 6D. The end of the ENPB-CPC was sealed by slow rotation of the balloon delivery tube. After that, the instruments were withdrawn, and CPC was restrained within the ENPB (Figure 6E), as was the case in the rabbit left thighbone.

2.10. X-ray Observation. Soft X-ray observation was performed using a Siemens Luminos Select X-ray. The observation was made using a standard projection on the operated limb, and the operational parameters were 43 kV, 2 mA, and 1.5 s.

2.11. Computed Tomography (CT) Imaging. At designated time points after implantation, the distribution of CPC within the rabbit thighbones or pig vertebrae was radiographically examined by CT (Toshiba, Aquilion 16 CT, Tokyo, Japan) at 120 kV and 150 mA for 750 ms.

2.12. Histological Analysis. At designated time points, the rabbits or pigs were sacrificed, and the implantation segments were cut. The bone tissues were fixed with 4% paraformaldehyde for 24 h and washed with water for 12−24 h. Then, the fixed samples were dehydrated with a series of ethanol−water solutions (70%, 75%, 80%, 85%, 90%, 95%, and 100%) for 24 h per solution change. Subsequently, the samples were immersed in xylene for 2 h and embedded in PMMA. Longitudinal sections were cut to approximately 150 μm thickness using microtomes (SP1600, Leica, Heidelberg, Germany) equipped with sturdy tungsten carbide knives and subsequently ground and polished to a final thickness of approximately 40 μm. The thin sections of bone were then subjected to Van Gieson staining by picric acid magenta and observed using optical microscopy (Leica, DMI 4000B, Mannheim, Germany).

2.13. Statistical Analysis. The data are shown as the mean value ± standard deviation (SD) of the parallel experiments. Statistical comparisons were carried out using Student's t test. $p < 0.05$ was considered to be significant.

3. RESULTS

3.1. P(DLLA−CL) Nanofibers and ENPB Fabrication. An appropriate titanium alloy mold (Figure 1A, upper part) was applied to collect the P(DLLA−CL) nanofibers. The ENPBs were formed on the titanium alloy mold (Figure 1A, middle part). The ENPBs with a thickness of 0.15−0.2 mm were chosen and taken down from the titanium alloy mold. Compared with the ENPBs on the titanium alloy mold, the taken-down ENPBs showed some degree of shrinkage (the lower part of Figure 1A). As shown in Figure 1B, the ENPB scaffolds typically exhibited smooth and randomly distributed nanofibrous structures with a mean diameter of 371 ± 98 nm (n = 50).

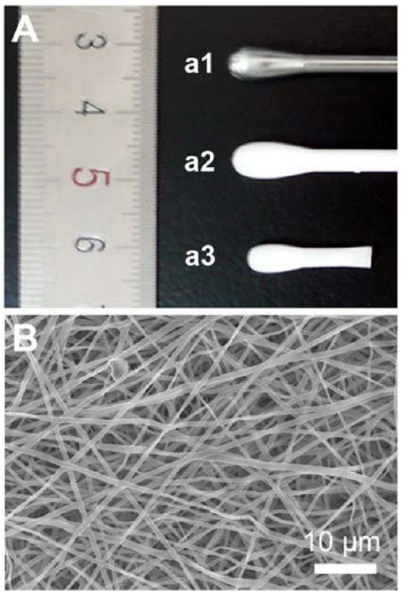

Figure 1. ENPB fabrication and SEM observations of P(DLLA−CL) nanofibers. (A) Fabrication of ENPBs: (a1) titanium alloy mold; (a2) ENPB formed on the titanium alloy mold; (a3) taken-down ENPB. (B) SEM micrograph of electrospun nanofibers in ENPBs.

3.2. In Vitro Biodegradation Behavior of ENPBs in Simulated Degradation Solutions. The physical and chemical properties of human serum are separated from the tissue microenvironment, which contains abundant lipases and other bioactivities. The lipase concentration in human serum is 0−160 U/L.[44] In some pathological conditions, the lipase concentration can be as high as 3000 U/L.[45] Proteinases also play pivotal roles in bone resorption and bone formation.[46,47] Therefore, five types of degradation solutions were used to study the in vitro degradation behaviors of ENPBs: SBF, a 100 U/L lipase solution, a 3000 U/L lipase solution, a 20 mg/mL proteinase K solution, and fresh human serum.

During the ENPB degradation process in fresh human serum, tiny cotton-like fragments appeared in the degradation solutions. The ENPB DR can be monitored by measuring the weight loss using an analytical balance.[48,49] The ENPB scaffold patches showed signs of degradation, and their DRs increased with time, as shown in Figure 2A. ENPB scaffold patches kept in a solution of SBF without a bioactivator (e.g., enzymes) had the lowest DR: they exhibited an approximate 15% DR at day 42. Faster DRs were shown in the other four degradation solutions, which contained bioactivators. The order of the final DRs for ENPBs in the five degradation solutions was as follows: a 3000 U/L lipase solution > human serum ≈ a 20 mg/mL proteinase K solution > a 100 U/L lipase solution > SBF. This order indicated that lipases might be the major degradation enzymes for ENPBs and that the DR could be regulated by the amount of lipases present.

ENPBs in human serum (Figure 2B) also exhibited morphological changes, as observed by SEM. At day 1, the ENPB scaffolds exhibited typical smooth and randomly distributed nanofibrous structures with a mean diameter of 356 ± 78 nm (n = 50), which was almost the same as that of untreated ENPB scaffolds (Figure 1B). With time, the P(DLLA−CL) nanofibers interblended. Finally, any remaining poriferous features were completely replaced with original nanofibers at day 42. Therefore, during degradation of the ENPBs, the ENPB nanofibers interblended with each other.

The tensile properties of ENPBs in fresh human serum as a function of the degradation time are shown in Figure 2C,D. Both the tensile strain at break (%) and the tensile stress at break (MPa) decreased with time. The trends are consistent with those observed in a lipase solution.[26] Moreover, they showed significant decreases ($p < 0.05$) after day 14, which might have resulted from polymer degradation (Figure 2A).

3.3. In Vitro Cell Biocompatibility Measurements of ENPB Scaffolds. To investigate the in vitro cell biocompatibility of ENPBs, three cell lines were employed: human osteosarcoma cells (MG63), mouse osteoblasts (MC 3T3-E1), and mouse embryonic fibroblasts (NIH 3T3).

Using CLSM, the amounts and distributions of cells grown on the ENPB scaffolds could be clearly observed (Figure 3A). As judged by the number of nuclei (indicated in blue), the cell

DOI: 10.1021/acsami.5b04868
ACS Appl. Mater. Interfaces 2015, 7, 18540−18552

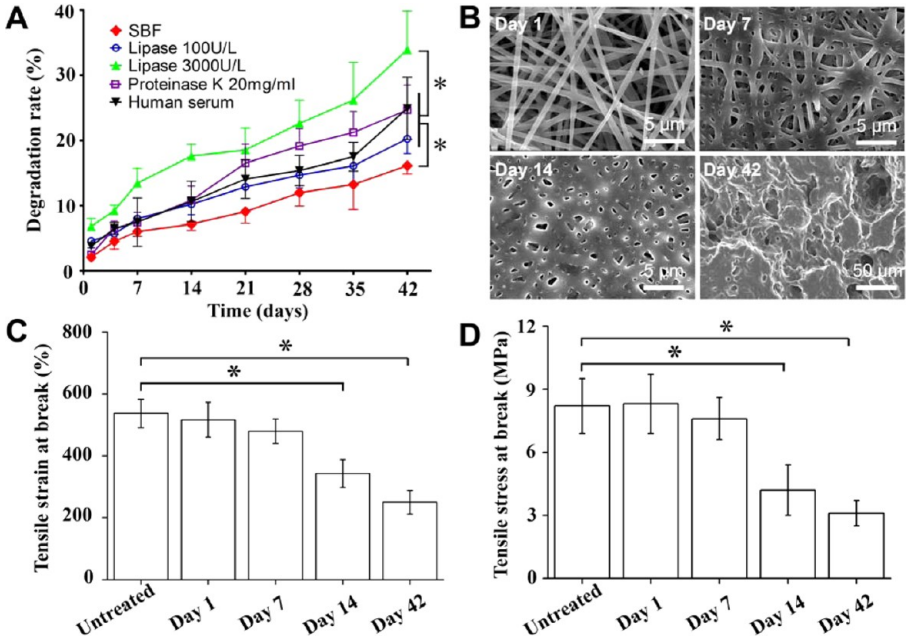

Figure 2. In vitro biodegradation behaviors of ENPB scaffolds in simulated degradation solutions at 100 rpm at 37 °C. (A) DR over time following incubations in five simulated degradation solutions: SBF, a 100 U/L lipase solution, a 3000 U/L lipase solution, a 20 mg/mL proteinase K solution, and fresh human serum. The DR was calculated according to eq 1. *: $p < 0.05$. (B) SEM micrographs of ENPB scaffolds after incubation in fresh human serum. (C) Tensile strain at break of ENPBs (%) over time following incubation in fresh human serum. *: $p < 0.05$. (D) Tensile stress at break (MPa) of ENPBs over time following incubation in fresh human serum. *: $p < 0.05$.

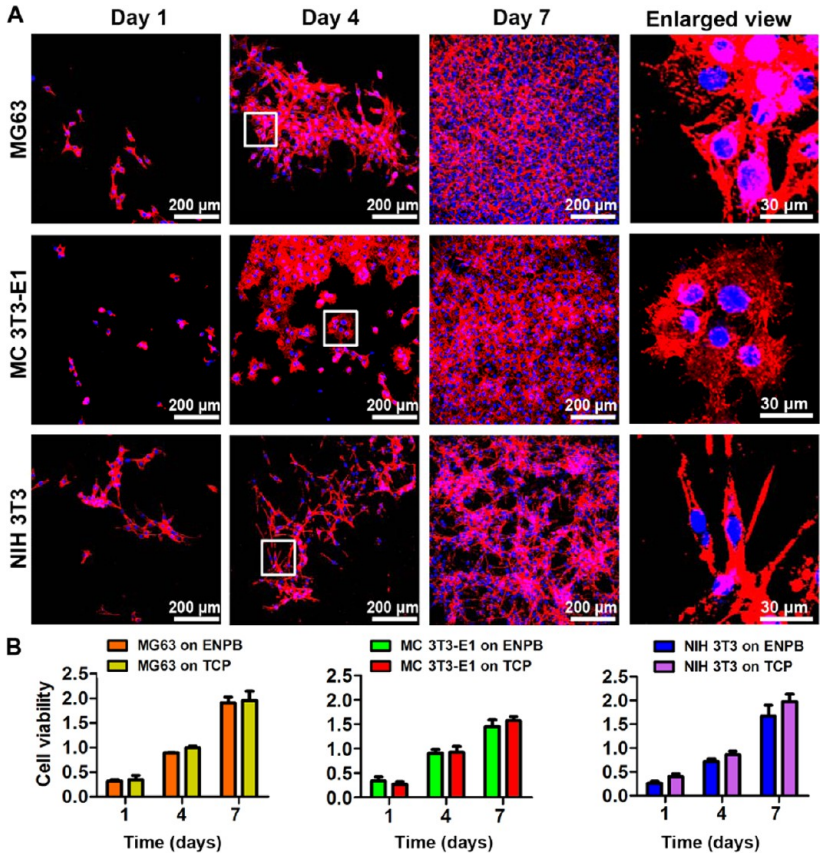

Figure 3. In vitro cell biocompatibility assays of ENPB scaffolds with MG63, MC 3T3-E1, and NIH 3T3 by CLSM observation and CCK-8 assay. (A) CLSM observation of cells grown on ENPB scaffolds on different incubation days. Nuclei are indicated in blue. Actin is indicated in red. The enlarged-view images correspond to the rectangles in the CLSM images taken on day 4. (B) CCK-8 assays of cell proliferation on ENPB scaffolds versus on TCPs. Inoculum cell density: 1×10^4 cells/well. Six parallel experiments for each sample ($n = 6$).

DOI: 10.1021/acsami.5b04868
ACS Appl. Mater. Interfaces 2015, 7, 18540−18552

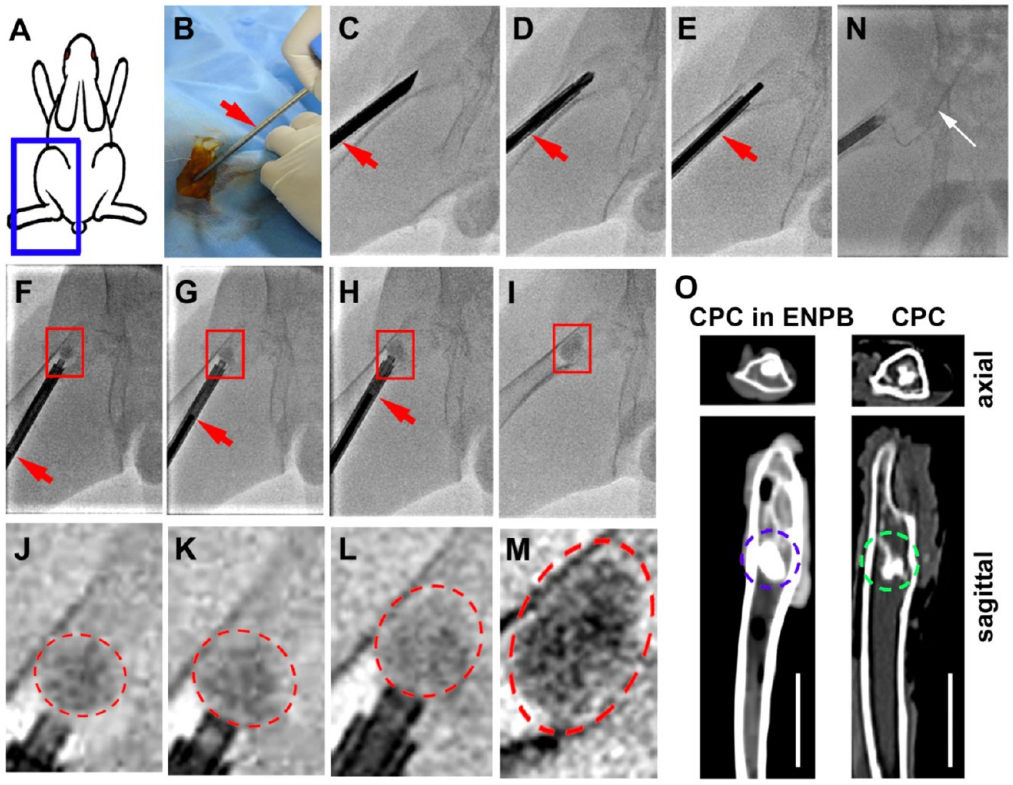

Figure 4. Implantation of ENPB-CPC and in vivo separation behaviors in rabbit thighbone. (A–M) Implantation of ENPB-CPC under DSA. (A) Illustration of the surgical site on the left thighbone of a rabbit. (B) Digital camera image of a punctured left rabbit thighbone made via a skin incision trocar with a diameter of 4.0 mm. (C) DSA image of the skin incision trocar in the punctured left rabbit thighbone. (D) DSA image of a bone drill in the skin incision trocar for drilling a circular hole as a working channel. (E) DSA image of a balloon delivery tube carrying ENPB in the skin incision trocar. (F–I) DSA images of ENPB inflation during the process of CPC injection. (J–M) Enlarged-view images from parts F–I, respectively. Red dashed ovals indicate ENPB inflation during CPC injection. (N) In three rabbits of the CPC group, collapsed CPC diffused into the inferior vena (indicated by the white arrow) via the iliac veins during CPC injection into the left rabbit thighbone. (O) CT images of CPC in an ENPB and CPC in rabbit thighbone on day 1. The CPC in the ENPB possesses a white rectangular shape (indicated by the blue circle). The CPC with no ENPB shows a dispersed and irregular shape (indicated by the red circle). The white scale bars at the right-bottom corner indicate 2 cm.

lines exhibited distinct growth patterns on the ENPB scaffold patches over time, and after 7 days of incubation, the cells almost completely covered the ENPB scaffold patches. According to actin staining (indicated in red), the ENPB scaffold patches did not obviously affect the cell shapes: the MG63 and MC 3T3-E1 lines were irregularly shaped, while the NIH 3T3 cells were spindle-shaped. These results demonstrated that the ENPB scaffolds did not hinder the cell proliferation and did not change the cell shape.

The activities of cells grown on the ENPB scaffolds and those grown on TCPs were studied by CCK-8 assay after 1, 4, and 7 days of incubation (Figure 3B). There were no differences in the signals corresponding to the ENPB scaffolds and the TCPs for any of the cell lines ($p > 0.05$). The CCK-8 assay quantitatively showed that the ENPB scaffolds fostered good cell proliferation ability for all three types of cells.

The morphologies of the cells grown on the ENPB scaffolds were observed by SEM, as shown in Figure S1. The three cell lines exhibited distinct growth patterns on the ENPB scaffold patches over time, and after 7 days of incubation, the cells almost completely covered the ENPB scaffolds, which is consistent with the CLSM results (Figure 3A). The cells did not produce an obvious effect on the ENPB nanofibers, even after 7 days of incubation. In addition, the ENPB scaffold patches did not obviously affect the cell shapes: the MG63 and MC 3T3-E1 cells were irregularly shaped, whereas the NIH 3T3 cells were spindle-shaped. These results are also consistent with the CLSM results.

In summary, three different cell lines proliferated well on the ENPB scaffolds, and no obvious differences were observed between them. Therefore, ENPBs possess good in vitro cytocompatility for the MG63, MC 3T3-E1, and NIH 3T3 cell lines.

3.4. Implantation of CPC or ENPB-CPC into Rabbit Thighbones. Under DSA, either ENPB-CPC or CPC was implanted into the left thighbone marrow cavities of rabbits using minimally invasive surgery, as shown in Figure 4. To evaluate the in vivo behaviors of ENPBs, commercial CPC was used in this work. Although the ENPBs were not visible, CPC was visible under DSA. The inflation of the ENPBs during the process of CPC injection was clearly observed (Figure 4F–I,J–M), which demonstrated that the CPC was restrained within the ENPBs. CPC collapsibility occurred in approximately 11% (3/27) of the rabbits during surgery. The collapsed CPC diffused into the inferior vena (indicated by a white arrow in Figure 4N) via the iliac veins during CPC injection into the left rabbit thighbone, which resulted in the death of the rabbits. Therefore, the ENPBs are capable of separating CPC from the surrounding bone microenvironments and can minimize the water-induced collapsibility of CPC.

At 24 h after surgery, the left rabbit thighbones were observed using CT, as shown in Figure 4O. In the CT scans,

DOI: 10.1021/acsami.5b04868
ACS Appl. Mater. Interfaces 2015, 7, 18540–18552

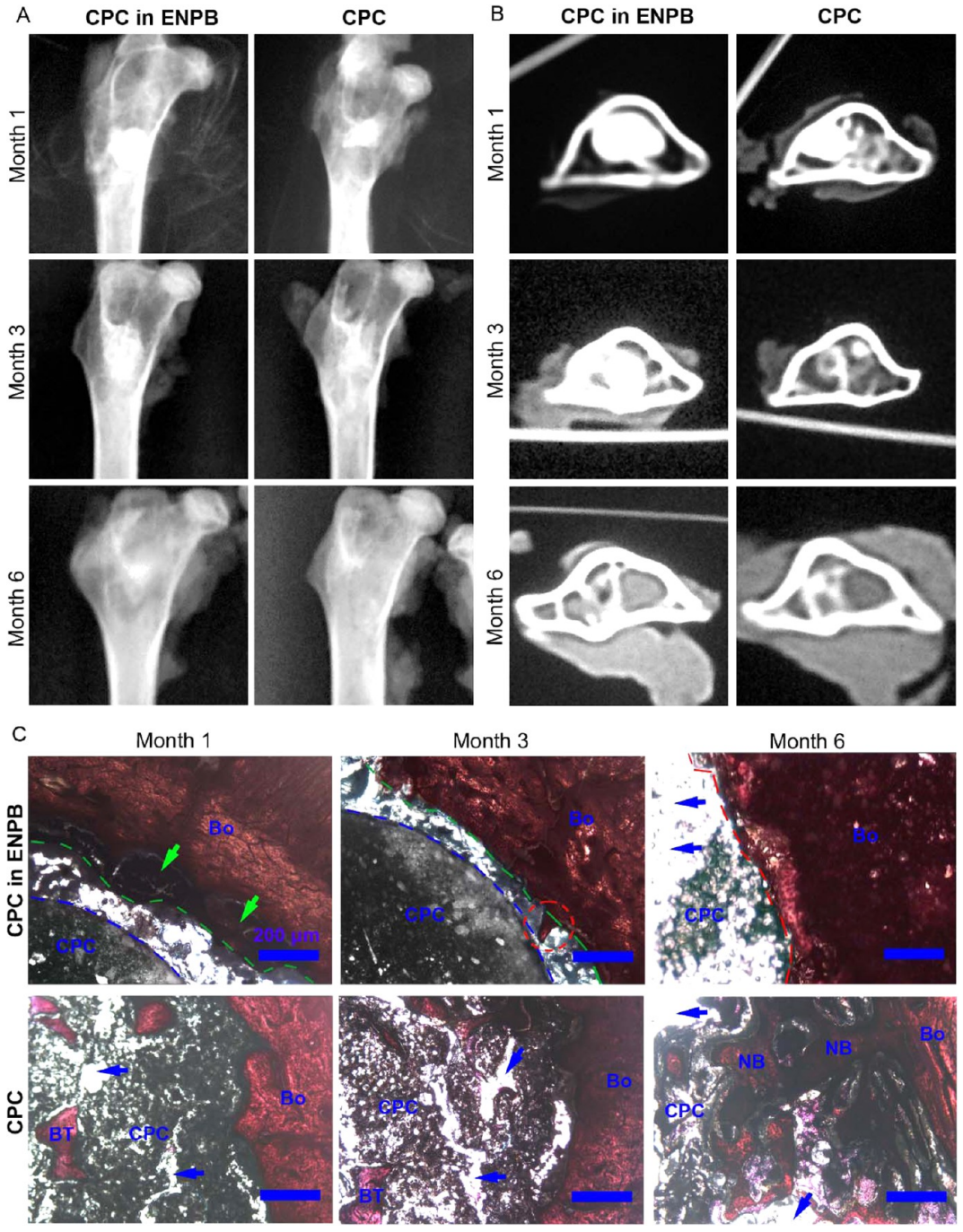

Figure 5. In vivo effects caused by ENPB-CPC or CPC implantation into rabbit thighbone. (A) X-ray images of rabbit thighbones at 1, 3, and 6 months postimplantation. The white areas in the rabbit thighbone marrow cavity are CPC. (B) CT images of rabbit thighbones at 1, 3, and 6 months postimplantation. The white areas in the rabbit thighbone marrow cavity are CPC. (C) Histological observation of rabbit thighbones at 1, 3, and 6 months postimplantation: Bo, bone; NB, new bone; BT, bone trabecula. The green dashed lines indicate the edges between the bone and the ENPB. The blue dashed lines indicate the edges between the CPC and the ENPB. The blue arrows indicate the gaps formed by CPC degradation (body-fluid-induced collapsibility). The red dashed circle indicates new bone that formed and entered into the ENPB. The green arrows indicate the collapsed bone trabeculas. The blue scale bars are 200 μm.

CPC present within the ENPB exhibited a white rectangular shape measuring approximately 9 mm × 6 mm (length × width, indicated by the dashed blue circle in the image). Free CPC (not in an ENPB) had a dispersed and irregular shape (indicated by the dashed green circle in the image). The CT results showed that ENPBs could separate CPC from the surrounding bone microenvironments in vivo, which is consistent with the DSA results (Figure 4F–I,J–M).

3.5. In Vivo Behaviors of CPC and ENPB-CPC in Rabbit Thighbones. At 1, 3, and 6 months after surgery, X-ray observation, CT observation, and histological analyses were employed to assess the in vivo behaviors of the CPC group versus the ENPB-CPC group in the rabbit left thighbone, as shown in Figure 5.

For the CPC group, the X-ray and CT images at 1 month showed that CPC was present in cortical bone. The X-ray and

DOI: 10.1021/acsami.5b04868
ACS Appl. Mater. Interfaces 2015, 7, 18540–18552

CT images showed that CPC degraded with time (Figure 5A,B). The histological image at 1 month showed that some gaps formed in the area around the CPC (indicated by blue arrows), which might be a result of CPC degradation (body-fluid-induced collapsibility). In addition, new bone formed and integrated into the CPC area over time. Some gaps were still apparent in the CPC area, as indicated by blue arrows. These results implied that the CPC degradation speed was greater than the speed of new bone formation in the rabbit thighbone marrow cavity, which is consistent with previous results from CPC implantation into the vertebral body.[50]

For the ENPB-CPC group, the X-ray and CT images showed that ENPB-CPC was present in cortical bone. Moreover, the degradation of ENPB-CPC was less than that of CPC group (Figure 5A,B). Histological image analysis at 1 month showed ENPBs with ring features separating the bone and the CPC, and the rings curved toward the CPC. These results also confirmed that CPC was restrained by the ENPBs. All of the bone trabeculas surrounding the ENPBs were collapsed (indicated by green arrows), which demonstrated that ENPB-CPC exerted pressure on the surrounding bone microenvironment. In addition, almost no gaps were present in the CPC area, which might be a result of the space constraint imposed by the ENPBs. By month 3, the ENPB scaffolds had degraded and new bones (indicated by the red dashed circle) formed that had taken in the ENPBs. By month 6, the ENPB scaffolds disappeared, which was consistent with the X-ray and CT images. Compared with CPC implantation, ENPB-CPC exerted more pressure on the surrounding bone microenvironment, enough to crush trabecular bone. Moreover, the use of ENPBs as CPC-filled containers delayed the CPC degradation (body-fluid-induced collapsibility).

3.6. Implantation of CPC or ENPB-CPC into Pig Vertebrae. Under digital DSA, ENPB-CPC or CPC was implanted into L2−L5 pig vertebrae using minimally invasive surgery, as shown in Figure 6. As shown in Figure 6B−D, ENPB-CPC and CPC were implanted into L5 and L4 vertebrae, respectively. In the ENPB-CPC group, the inflated ENPB-CPC was spindle-shaped and had a diameter of 6.7 ± 0.5 mm (n = 6; L5 vertebra in Figure 6D,E), which was larger than the inner diameter of the working channel (4.0 mm). This suggested that the inflated ENPB could exert pressure on and crush the surrounding trabecular bone. In the CPC group, the CPC was randomly dispersed and had a diameter of 8.2 ± 0.8 mm (n = 6; L4 vertebra in Figure 6D,E), which was larger than the inner diameter of the working channel (4.0 mm) and the diameter of the inflated ENPB-CPC (6.7 ± 0.5 mm). This suggested that CPC was dispersed into the surrounding trabecular bone and that the ENPBs could separate CPC from the surrounding bone microenvironments.

3.7. In Vivo Behaviors of CPC and ENPB-CPC in Pig Vertebrae. CT scanning (Figure 7A−D) and histological analyses (Figure 7E−H) were employed to assess the in vivo behaviors of the CPC and ENPB-CPC groups in pig vertebrae.

In the CPC group, CT scanning showed that CPC collapsibility occurred in approximately 1 out of 12 pig vertebrae at 1 month after surgery (indicated by the yellow arrow in Figure 7A). The CPC dispersed throughout the pig vertebrae (L2 and L4 vertebrae in Figure 7B) at 3 month after surgery. Finally, both the CPC and the working channels disappeared, and the treated vertebrae (Figure 7C) showed no obvious differences from the untreated vertebrae (Figure 7D). Histological images showed that the working channel (the empty circle area indicated by a black asterisk in Figure 7G) disappeared at 6 month after surgery (Figure 7H). Therefore, although CPC collapsibility was uncontrollable, the CPC group showed good new bone formation ability.

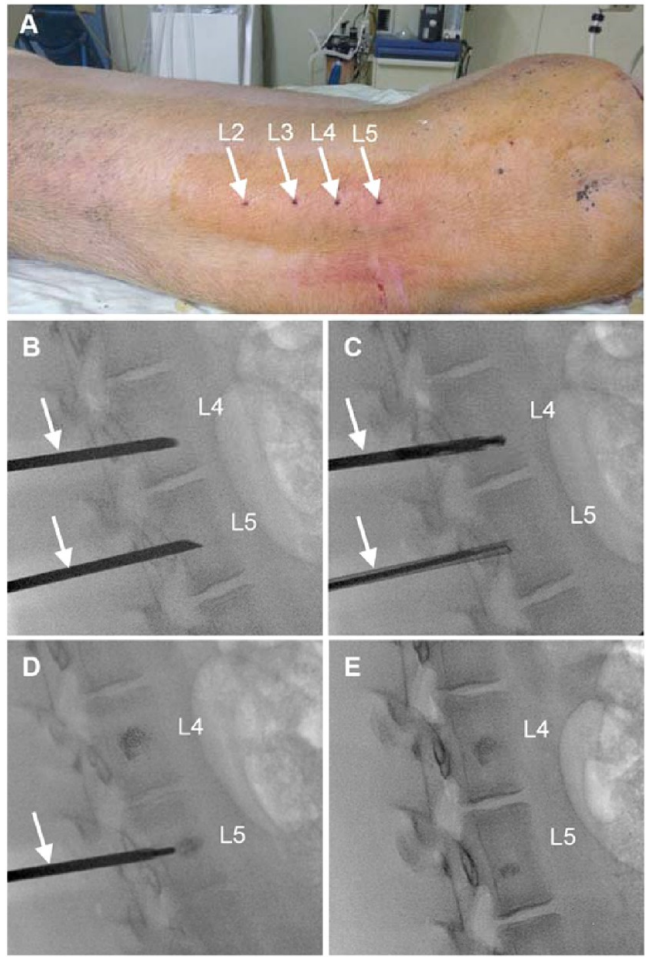

Figure 6. Implantation of ENPB-CPC or CPC into pig vertebrae. (A) Digital image of the surgical area after the implantation. (B) Placement of the skin incision trocar in the L4 and L5 vertebrae. (C) The bone drill was placed in the skin incision trocar to drill a circular hole to serve as a working channel in the L4 vertebra. The needle of the skin incision trocar in the L5 vertebra was removed. (D) CPC dispersed in L4 vertebra after CPC injection and removal of the skin incision trocar. CPC injection into an ENPB, which is tied onto a balloon delivery tube in the L5 vertebra. (E) ENPB-CPC in the L5 vertebra after CPC injection and removal of the balloon delivery tube and the skin incision trocar. The outer diameter of the skin incision trocar (indicated by white arrows) was 4 mm.

In the ENPB-CPC group, CT scanning showed that the CPC area increased with time (L3 and L5 vertebrae in Figure 7A,B), which implied that ENPB degraded and CPC dispersed into the trabecular bone. Finally, both CPC and the working channels disappeared, and the treated vertebrae (Figure 7C) showed no obvious difference from the untreated vertebrae (Figure 7D). The CPC area in the ENPB-CPC group was less than that in the CPC group at 3 month after surgery, which suggested that ENPB delayed CPC degradation. Histological images showed that the working channel (the empty circle area, indicated by a black asterisk in Figure 7E) disappeared by 6 month after surgery (Figure 7F). Therefore, the ENPB-CPC group showed good new bone formation ability. It should be

DOI: 10.1021/acsami.5b04868
ACS Appl. Mater. Interfaces 2015, 7, 18540−18552

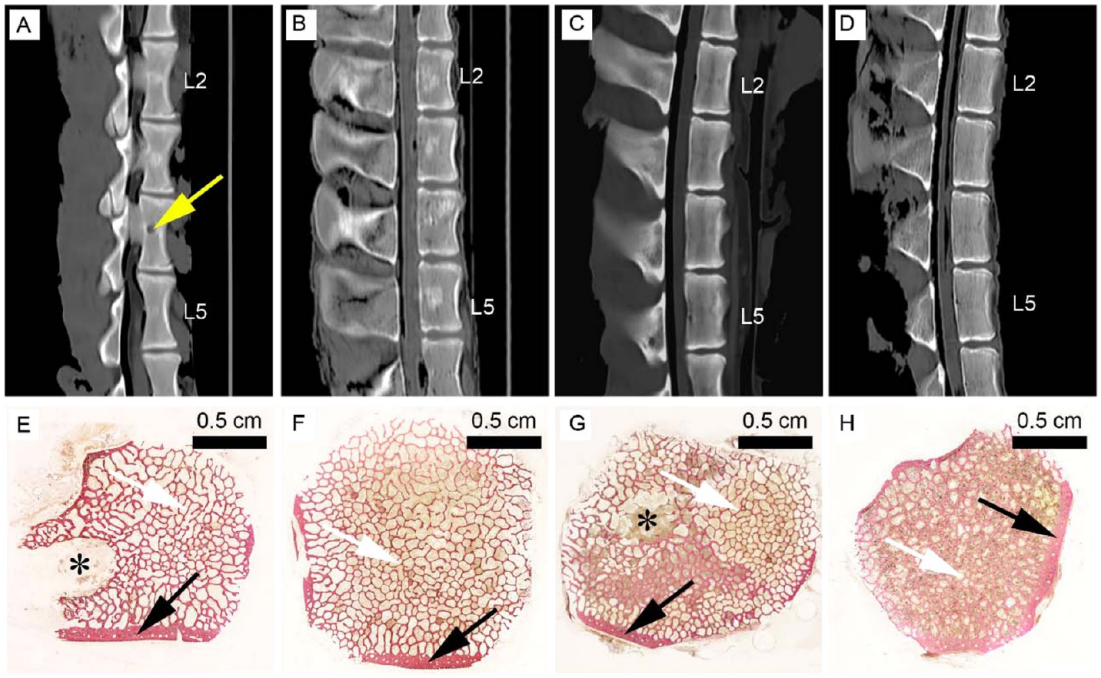

Figure 7. In vivo effects caused by ENPB-CPC and CPC implantation in pig vertebrae. (A–C) CT images of pig vertebrae at 1, 3, and 6 months postimplantation. The yellow arrow indicates an empty working channel without CPC, which implied CPC collapsibility. L2 and L5 indicate L2 vertebrae and L5 vertebrae, respectively. (D) CT image of pig vertebrae after 6 months in a culture without implantation. (E and F) Histological observation of pig vertebrae at 3 and 6 months postimplantation in the ENPB-CPC group. The black asterisk indicates the working channel. The white arrows indicate bone trabecula. The black arrows indicate bone cortex. (G and H) Histological observation of pig vertebrae at 3 and 6 months postimplantation in the CPC group. The black asterisk indicates the working channel. The white arrows indicate bone trabecula. The black arrows indicate bone cortex.

noted that the bone trabeculas formed a round circle around the ENPB by 3 month after surgery, which was not observed in the CPC group. This suggusted that new bone formed around the ENPB, which might have resulted from the release of calcium from the CPC in the ENPB to the trabecular bone.

4. DISCUSSION

To explore the use of CPC in the treatment of VCFs, we recently developed ENPBs using an electrospinning technique.[26] Before moving to clinical application, the in vitro and in vivo behaviors of the ENPBs were systematically evaluated in this work. This work will also be of benefit to the development of polymer-based medical implants in the future.

4.1. In Vitro and in Vivo Separation Behavior of ENPBs. Our previous in vitro work showed that ENPBs could be inflated by injection of CPC and could separate CPC from the surrounding ambient environment.[26] In this work, the in vivo observation of ENPB-CPCs showed that the ENPBs separated CPC from the surrounding bone microenvironments in rabbit thighbones (Figure 4) and pig vertebrae (Figure 6). Without the use of ENPB, CPC could occasionally collapse and diffuse into the inferior vena (indicated by the white arrow in Figure 4N) in rabbit thighbones. Moreover, CPC collapsibility in the CPC group also occasionally occurred in pig vertebrae at 1 month after surgery (indicated by the yellow arrow in Figure 7A). Therefore, ENPBs delayed the in vivo CPC degradation (body-fluid-induced collapsibility) in rabbit thighbones and pig vertebrae. These results confirmed that ENPBs could separate CPC from the surrounding bone microenvironment in vitro and in vivo and therefore could prevent the water-induced collapsibility of CPC and minimize CPC leakage in vivo.

4.2. Pressure Exerted by ENPBs on the Surrounding Bone Microenvironment in Vitro and in Vivo. The load-bearing ability of an ENPB filled with CPC in restoring the height of a fractured vertebral body depends on both the mechanical properties of the CPC and the burst pressure of the ENPB. If the ENPB does not burst during CPC injection into ENPB, then it will become inflated and restore the height of the fractured vertebral body before CPC solidifies to stabilize the height restoration. If an ENPB has a low burst pressure and therefore bursts during CPC injection, then CPC will distribute in trabecular bone, and the height of the fractured vertebral body cannot be restored. Our previous work demonstrated that ENPB-CPC had a high average burst pressure of 15.2 ± 0.8 atm in vitro.[26] The average inflation pressure of commercial inflatable bone tamps to restore the fractured vertebral body height is 9 atm (range 5–17 atm).[26] Therefore, theoretically, the ENPBs satisfied the load-bearing ability required for the treatment of VCFs. The inflated ENPB-CPC could exert pressure on the surrounding materials when more and more CPC was injected into the ENPBs. In this work, an in vivo histological observation of rabbit thighbone showed that the bone trabeculas were destroyed by ENPB-CPC (indicated by the green arrows in Figure 5). The in vivo implantation process in pig vertebrae also showed that the inflated ENPB-CPC was spindle-shaped and had a larger diameter than the working channel (Figure 6), which suggested that ENPB-CPC could exert enough pressure to crush the surrounding trabecular bone. This is a desired outcome for an ENPB-CPC because the crushed bone trabeculas can provide space for the inflated ENPB. Therefore, the ENPB-CPC exerted pressure on the surrounding bone microenvironment in rabbit thighbones and pig vertebrae. This finding also implied that ENPB-CPCs have

DOI: 10.1021/acsami.5b04868
ACS Appl. Mater. Interfaces 2015, 7, 18540–18552

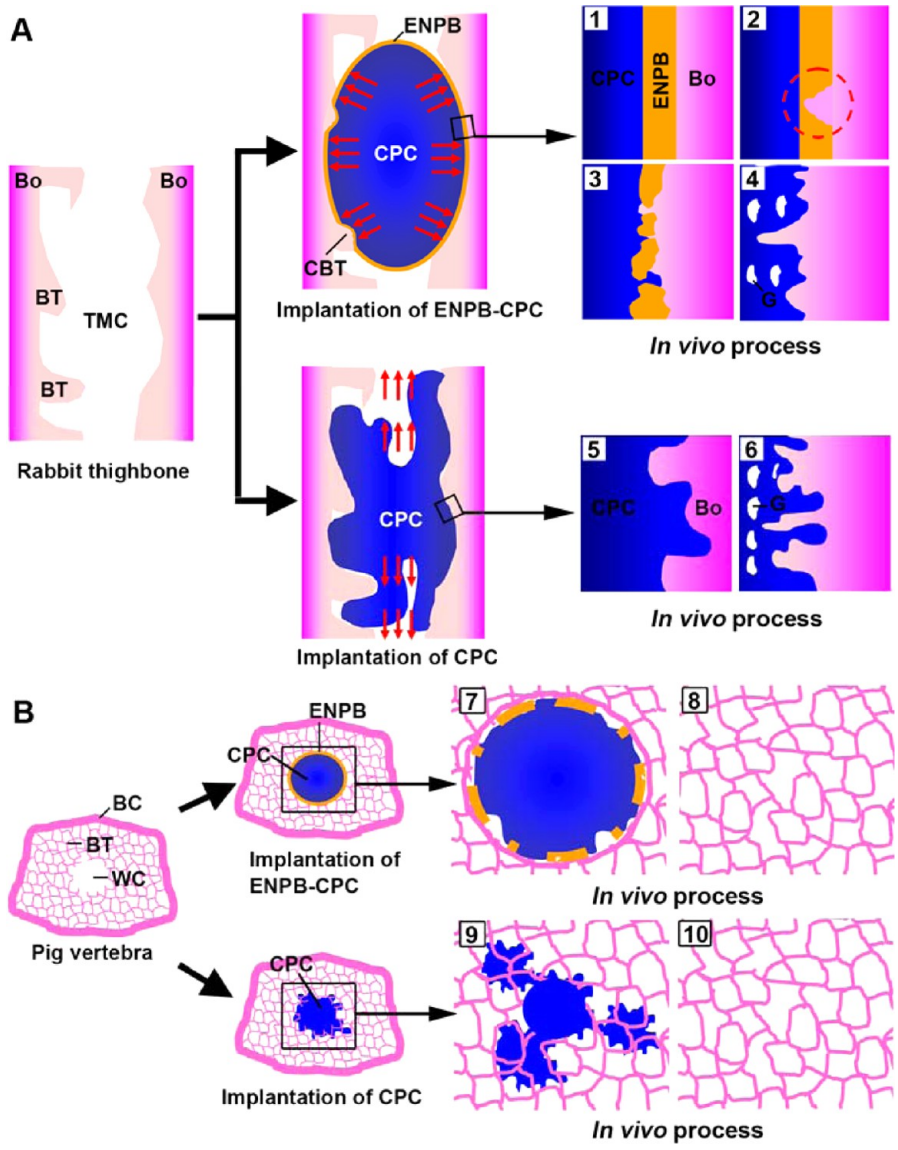

Figure 8. Proposed mechanisms behind the in vivo effects caused by ENPB-CPC and CPC implantation in rabbit thighbone (A) and pig vertebrae (B): TMC, thighbone marrow cavity; Bo, bone; BT, bone trabecula; BC, bone cortex; WC, working channel; CBT, crushed bone trabecula; G, gaps formed by CPC degradation. (1−4) Possible in vivo process of ENPB-CPC in rabbit thighbone. (5 and 6) Possible in vivo process of CPC in rabbit thighbone. (7 and 8) Possible in vivo process of ENPB-CPC in pig vertebra. (9 and 10) Possible in vivo process of CPC in pig vertebra.

load-bearing ability in vivo and therefore might be able to restore the height of a fractured vertebral body. However, the pressure in vivo depends on several factors, such as the sealing condition of the ENPBs and the amount of CPC that is filled into the container. Thus, knowing an exact and actual pressure could provide more detailed information regarding the biomechanical characteristics involved in crushing the trabecula. The sealing method in this work is not desirable when high pressure is needed to restore the height of a fractured vertebral body. Therefore, it is necessary to develop sealing devices that can improve the sealing conditions.[51]

4.3. In Vitro and in Vivo Degradation Behavior of ENPBs. In this work, the results from in vitro degradation experiments showed that ENPBs could be degraded in several simulated degradation solutions (Figure 2A). The order of the final DRs for ENPBs in the 5 tested degradation solutions was as follows: a 3000 U/L lipase solution > human serum ≈ a 20 mg/mL proteinase K solution > a 100 U/L lipase solution > SBF. Moreover, during ENPB degradation, the ENPB nanofibers interblended over time (Figure 2B), which might have induced the decreases in their tensile strain at break (Figure 2C) and tensile stress at break (Figure 2D). In vivo degradation of the ENPBs was also observed by 3 months after surgery in rabbit thighbones (Figure 5C) and pig vertebrae (Figure 7E,F). All of these results showed that the use of ENPBs simply shifted the problem to a later time point rather than overcoming it. Therefore, the biodegradation of ENPBs ensured that the surrounding bones were slowly exposed to CPC.

4.4. In Vitro Cell Proliferation Ability and in Vivo New Bone Formation Ability of ENPBs. P(DLLA−CL) is formed from a synthetic polymerization of D-lactic acid, L-lactic acid, and caprolactone monomers and widely used in tissue engineering and regenerative medicine.[52−56] Thus far, P(DLLA−CL) biomaterials have been proven to impart good in vitro proliferation ability to liver cells,[57] nerve cells,[58]

DOI: 10.1021/acsami.5b04868
ACS Appl. Mater. Interfaces 2015, 7, 18540−18552

schwann cells,[59] and osteoblasts.[60,61] Our work also revealed that three types of cells, including MC 3T3-E1, MG63, and NIH 3T3, could grow well on P(DLLA−CL) nanofibers (Figures 3 and S1). The most relevant primary cells in the bone tissue microenvironment are bone marrow stromal cells. Therefore, it is necessary to further study the in vitro cell biocompatibility of ENPBs using the most relevant primary cells. However, our work has already initially demonstrated that ENPBs have good in vitro cell biocompatibility.

The induction of new bone formation after ENPB-CPC implantation in the rabbit marrow cavity was observed by histological analysis (Figure 5C). New bone formed with degradation of the ENPBs. Compared with direct CPC implantation, the use of ENPBs as CPC-filled containers delayed CPC degradation (body-fluid-induced collapsibility) in rabbit thighbones and pig vertebrae. Hence, the use of ENPBs leads to robust in vivo bone cell proliferation, which was consistent with the in vitro cell proliferation results.

4.5. Possible Mechanisms of the in Vivo Effects Caused by ENPB-CPC or CPC Implantation in Rabbit Thighbones and Pig Vertebrae. On the basis of our results and the above analysis, we can propose the possible mechanisms behind the in vivo effects that result from ENPB-CPC or CPC implantation in rabbit thighbones (Figure 8A) and pig vertebrae (Figure 8B).

The possible mechanism to explain the in vivo effects caused by CPC implantation in the rabbit thighbone marrow cavity is shown in the lower half of Figure 8A. After CPC injection, CPC diffused into the bone marrow cavity. As time passed, CPC degraded, and several gaps (indicated by G) formed in the CPC area. Meanwhile, new bone formed and was interated into the CPC area. Moreover, the CPC degradation speed was greater than the new bone formation speed, leading to the formation of gaps in the CPC area.

The possible mechanism behind the in vivo effects caused by ENPB-CPC implantation in the rabbit thighbone marrow cavity is shown in the upper half of Figure 8A. After the injection of CPC into an ENPB in the rabbit thighbone marrow cavity, CPC was restrained within the ENPB. The ENPB-CPC exerted pressure on the surrounding bone microenvironment, which was enough to crush the trabecular bone (indicated by CBT). As time passed, the ENPB degraded, and new bone formed. After the ENPB degraded, the CPC degradation speed was greater than the new bone formation speed, leading to the formation of gaps in the CPC area.

The possible mechanism behind the in vivo effects caused by CPC implantation in pig vertebrae is shown in the lower half of Figure 8B. After the CPC injection, CPC diffused into the working channel area and into the spaces in the trabecular bone. As time passed, CPC degraded and diffused into the spaces in the trabecular bone. Meanwhile, new trabecular bone formed and integrated into the CPC area (the working channel area). Finally, by 6 months after surgery, any sign of the previous working channel area disppeared.

The possible mechanism behind the in vivo effects caused by ENPB-CPC implantation in pig vertebrae is shown in the upper half of Figure 8B. After the injection of CPC into an ENPB in the working channel area, CPC was restrained within the ENPB. The resultant ENPB-CPC exerted pressure on the surrounding bone microenvironment, which was enough to crush the trabecular bone and enlarge the working channel area. As time passed, the ENPB degraded, and new trabecular bone formed around the ENPB-CPC. Finally, by 6 months after surgery, any sign of the previous working channel area disappeared.

5. CONCLUSION

In previous work, we developed ENPBs and tested them in vitro to prove that they could separate CPC from surrounding environments and that they possessed sufficient load-bearing ability to restore the height of a fractured vertebral body in VCFs. However, our previous work did not systematically compare the in vitro and in vivo effects caused by using ENPBs as CPC-filled containers, which is important to assess prior to engaging in clinical research. In this work, the separation, pressure, degradation, and new bone formation effects caused by ENPBs in vitro and in vivo (rabbit thighbones and pig vertebrae) were systematically analyzed and compared. ENPBs could separate CPC from the surrounding bone microenvironment both in vitro and in vivo. ENPB-CPCs exerted pressure on the surrounding bone microenvironment, which was enough to crush trabecular bone. Compared with the CPC implantation, the use of ENPBs as CPC-filled containers delayed the CPC degradation (body-fluid-induced collapsibility). Finally, possible mechanisms to explain the in vivo effects caused by ENPB-CPC and CPC implantation in rabbit thighbones and pig vertebrae were proposed. Our work suggests that ENPBs can be potentially used as CPC-filled containers and provides an experimental basis for the clinical application of ENPBs for the treatment of VCFs in the future. In addition, our work also demonstrated that the ENPB behaviors varied in different bone microenvironments. Finally, our work will be of benefit to the development of P(DLLA−CL)-based medical implants in the future.

■ ASSOCIATED CONTENT

Supporting Information

The Supporting Information is available free of charge on the ACS Publications website at DOI: 10.1021/acsami.5b04868.

In vitro cell biocompatibility assays of ENPB scaffolds with MG63, MC 3T3-E1, and NIH 3T3 measured by SEM (PDF)

■ AUTHOR INFORMATION

Corresponding Authors

*E-mail: cjr.sungang@vip.163.com (G.S.).
*E-mail: jianzhongpku@hotmail.com (J.Zhong).
*E-mail: hdn_nercn@163.com (D.H.).

Author Contributions

§Both authors contributed equally to the work.

Author Contributions

G.S., J.Zhong, and D.H. led the research. J.Zhong and G.S. designed the research. X.L., J.Zhong, M.M., J.Zhou, X.P., and Y.Y. performed the research and collected the data. J.Zhong, X. L., and D.W. analyzed the data. J.Zhong and D.W. wrote the paper.

Notes

The authors declare no competing financial interest.

■ ACKNOWLEDGMENTS

This research has been supported by research grants from the National High Technology Research and Development Program of China (863 Program 2013AA032203), the National Natural Science Foundation of China (Grants 51073173 and

DOI: 10.1021/acsami.5b04868
ACS Appl. Mater. Interfaces 2015, 7, 18540−18552

51203024), the Shanghai Pujiang Talent Program (12PJ1430300), the Special Fund for Talents in Minhang District of Shanghai (2012), and the Director Fund of Jinan Military General Hospital (Grant 2012ZX002).

REFERENCES

(1) Silverman, S. L.; Minshall, M. E.; Shen, W.; Harper, K. D.; Xie, S. Health-Related Quality of Life Subgroup of the Multiple Outcomes of Raloxifene Evaluation, S. The Relationship of Health-Related Quality of Life to Prevalent and Incident Vertebral Fractures in Postmenopausal Women with Osteoporosis: Results from the Multiple Outcomes of Raloxifene Evaluation Study. *Arthritis Rheum.* **2001**, *44*, 2611−2619.

(2) Silverman, S. L. The Clinical Consequences of Certebral Compression Fracture. *Bone* **1992**, *13*, S27−S31.

(3) Lau, E.; Ong, K.; Kurtz, S.; Schmier, J.; Edidin, A. Mortality Following the Diagnosis of a Vertebral Compression Fracture in the Medicare Population. *J. Bone Jt. Surg., Am. Vol.* **2008**, *90*, 1479−1486.

(4) Huntoon, M. Vertebral Compression Fractures in Elderly Osteoporosis Patients Receiving Glucocorticoid Intra-Articular Injections. *Pain Pract.* **2006**, *6*, 206−211.

(5) Garfin, S. R.; Buckley, R. A.; Ledlie, J. Balloon Kyphoplasty Outcomes, G. Balloon Kyphoplasty for Symptomatic Vertebral Body Compression Fractures Results in Rapid, Significant, and Sustained Improvements in Back Pain, Function, and Quality of Life for Elderly Patients. *Spine (Philadelphia)* **2006**, *31*, 2213−2220.

(6) Old, J. L.; Calvert, M. Vertebral Compression Fractures in the Elderly. *Am. Fam. Physician* **2004**, *69*, 111−116.

(7) Mathis, J. M.; Barr, J. D.; Belkoff, S. M.; Barr, M. S.; Jensen, M. E.; Deramond, H. Percutaneous Vertebroplasty: a Developing Standard of Care for Vertebral Compression Fractures. *AJNR Am. J. Neuroradiol.* **2001**, *22*, 373−381.

(8) Wardlaw, D.; Cummings, S. R.; Van Meirhaeghe, J.; Bastian, L.; Tillman, J. B.; Ranstam, J.; Eastell, R.; Shabe, P.; Talmadge, K.; Boonen, S. Efficacy and Safety of Balloon Kyphoplasty Compared With Non-Surgical Care for Vertebral Compression Fracture (FREE): a Randomised Controlled Trial. *Lancet* **2009**, *373*, 1016−1024.

(9) Tancioni, F.; Navarria, P.; Pessina, F.; Marcheselli, S.; Rognone, E.; Mancosu, P.; Santoro, A.; Baena, R. R. Early Surgical Experience with Minimally Invasive Percutaneous Approach for Patients with Metastatic Epidural Spinal Cord Compression (MESCC) to Poor Prognoses. *Ann. Surg. Oncol.* **2012**, *19*, 294−300.

(10) Morris, L. G.; Tran, T. N.; DeLacure, M. D. Early Experience with Minimally Invasive Esophagectomy in Head and Neck Surgical Patients. *Otolaryngol.–Head Neck Surg.* **2007**, *137*, 947−949.

(11) Hadjipavlou, A. G.; Tzermiadianos, M. N.; Katonis, P. G.; Szpalski, M. Percutaneous Vertebroplasty and Balloon Kyphoplasty for the Treatment of Osteoporotic Vertebral Compression Fractures and Osteolytic Tumours. *J. Bone Jt. Surg., Br. Vol.* **2005**, *87-B*, 1595−1604.

(12) Lieberman, I. H.; Togawa, D.; Kayanja, M. M. Vertebroplasty and Kyphoplasty: Filler Materials. *Spine J.* **2005**, *5*, S305−S316.

(13) Sun, Y. C.; Teng, M. M.; Yuan, W. S.; Luo, C. B.; Chang, F. C.; Lirng, J. F.; Guo, W. Y.; Chang, C. Y. Risk of Post-Vertebroplasty Fracture in Adjacent Vertebral Bodies Appears Correlated with the Morphologic Extent of Bone Cement. *J. Chin. Med. Assoc.* **2011**, *74*, 357−362.

(14) Frankel, B. M.; Monroe, T.; Wang, C. Percutaneous Vertebral Augmentation: an Elevation in Adjacent-Level Fracture Risk in Kyphoplasty as Compared with Vertebroplasty. *Spine J.* **2007**, *7*, 575−582.

(15) Voormolen, M. H.; Lohle, P. N.; Juttmann, J. R.; van der Graaf, Y.; Fransen, H.; Lampmann, L. E. The Risk of New Osteoporotic Vertebral Compression Fractures in the Year After Percutaneous Vertebroplasty. *J. Vasc. Interv. Radiol.* **2006**, *17*, 71−76.

(16) Turner, T. M.; Urban, R. M.; Singh, K.; Hall, D. J.; Renner, S. M.; Lim, T. H.; Tomlinson, M. J.; An, H. S. Vertebroplasty Comparing Injectable Calcium Phosphate Cement Compared with Polymethylmethacrylate in a Unique Canine Vertebral Body Large Defect Model. *Spine J.* **2008**, *8*, 482−487.

(17) Liu, C.; Shao, H.; Chen, F.; Zheng, H. Rheological Properties of Concentrated Aqueous Injectable Calcium Phosphate Cement Slurry. *Biomaterials* **2006**, *27*, 5003−5013.

(18) Ryu, K.-S.; Shim, J.-H.; Heo, H.-Y.; Park, C.-K. Therapeutic Efficacy of Injectable Calcium Phosphate Cement in Osteoporotic Vertebral Compression Fractures: Prospective Nonrandomized Controlled Study at 6-Month Follow-up. *World Neurosurg.* **2010**, *73*, 408−411.

(19) Bernhard, J.; Heini, P. F.; Villiger, P. M. Asymptomatic Diffuse Pulmonary Embolism Caused by Acrylic Cement: an Unusual Complication of Percutaneous Vertebroplasty. *Ann. Rheum. Dis.* **2003**, *62*, 85−86.

(20) Baroud, G.; Bohner, M.; Heini, P.; Steffen, T. Injection Biomechanics of Bone Cements Used in Vertebroplasty. *Biomed. Mater. Eng.* **2004**, *14*, 487−504.

(21) Zheng, Z.; Luk, K. D.; Kuang, G.; Li, Z.; Lin, J.; Lam, W. M.; Cheung, K. M.; Lu, W. W. Vertebral augmentation with a novel Vessel-X bone void filling container system and bioactive bone cement. *Spine (Philadelphia)* **2007**, *32*, 2076−2082.

(22) Rotter, R.; Martin, H.; Fuerderer, S.; Gabl, M.; Roeder, C.; Heini, P.; Mittlmeier, T. Vertebral Body Stenting: a New Method for Vertebral Augmentation Versus Kyphoplasty. *Eur. Spine J.* **2010**, *19*, 916−923.

(23) Xu, H. H. K.; Quinn, J. B.; Takagi, S.; Chow, L. C. Processing and Properties of Strong and Non-rigid Calcium Phosphate Cement. *J. Dent. Res.* **2002**, *81*, 219−224.

(24) Moreau, J. L.; Weir, M. D.; Xu, H. H. K. Self-Setting Collagen-Calcium Phosphate Bone Cement: Mechanical and Cellular Properties. *J. Biomed. Mater. Res., Part A* **2009**, *91A*, 605−613.

(25) Panzavolta, S.; Bracci, B.; Focarete, M. L.; Gualandi, C.; Bigi, A. Fiber Reinforcement of a Biomimetic Bone Cement. *J. Mater. Sci.: Mater. Med.* **2012**, *23*, 1363−1370.

(26) Sun, G.; Wei, D.; Liu, X.; Chen, Y.; Li, M.; He, D.; Zhong, J. Novel Biodegradable Electrospun Nanofibrous P(DLLA-CL) Balloons for the Treatment of Vertebral Compression Fractures. *Nanomedicine (N. Y., NY, U. S.)* **2013**, *9*, 829−838.

(27) Chen, B.-Y.; Wang, Y.-S.; Mi, H.-Y.; Yu, P.; Kuang, T.-R.; Peng, X.-F.; Wen, J.-S. Effect of Poly(Ethylene Glycol) on the Properties and Foaming Behavior of Macroporous Poly(Lactic Acid)/Sodium Chloride Scaffold. *J. Appl. Polym. Sci.* **2014**, *131*, 41181.

(28) Wen, Y.; Meng, W. S. Recent In Vivo Evidences of Particle-Based Delivery of Small-Interfering RNA (siRNA) into Solid Tumors. *J. Pharm. Innov.* **2014**, *9*, 158−173.

(29) Engman, C.; Wen, Y.; Meng, W. S.; Bottino, R.; Trucco, M.; Giannoukakis, N. Generation of Antigen-Specific Foxp3+ Regulatory T-cells In Vivo Following Administration of Diabetes-Reversing Tolerogenic Microspheres Does Not Require Provision of Antigen in the Formulation. *Clin. Immunol.* **2015**, *12*, 00094−00097.

(30) Yu, Z.; Paul, R.; Bhattacharya, C.; Bozeman, T. C.; Rishel, M. J.; Hecht, S. M. Structural Features Facilitating Tumor Cell Targeting and Internalization by Bleomycin and Its Disaccharide. *Biochemistry* **2015**, *54*, 3100−3109.

(31) Yu, Z.; Schmaltz, R. M.; Bozeman, T. C.; Paul, R.; Rishel, M. J.; Tsosie, K. S.; Hecht, S. M. Selective Tumor Cell Targeting by the Disaccharide Moiety of Bleomycin. *J. Am. Chem. Soc.* **2013**, *135*, 2883−2886.

(32) Wildemann, B.; Kandziora, F.; Krummrey, G.; Palasdies, N.; Haas, N.; Raschke, M.; Schmidmaier, G. Local and Controlled Release of Growth Factors (Combination of IGF-I and TGF-beta I, and BMP-2 Alone) from a Polylactide Coating of Titanium Implants Does Not Lead to Ectopic Bone Formation in Sheep Muscle. *J. Controlled Release* **2004**, *95*, 249−256.

(33) Schmidmaier, G.; Baehr, K.; Mohr, S.; Kretschmar, M.; Beck, S.; Wildemann, B. Biodegradable Polylactide Membranes for Bone Defect Coverage: Biocompatibility Testing, Radiological and Histological Evaluation in a Sheep Model. *Clin. Oral Implan. Res.* **2006**, *17*, 439−444.

DOI: 10.1021/acsami.5b04868
ACS Appl. Mater. Interfaces 2015, 7, 18540−18552

(34) Wheeler, D. L.; Chamberland, D. L.; Schmitt, J. M.; Buck, D. C.; Brekke, J. H.; Hollinger, J. O.; Joh, S. P.; Suh, K. W. Radiomorphometry and Biomechanical Assessment of Recombinant Human Bone Morphogenetic Protein 2 and Polymer in Rabbit Radius Ostectomy Model. *J. Biomed. Mater. Res.* **1998**, *43*, 365−373.
(35) Vertenten, G.; Lippens, E.; Gironès, J.; Gorski, T.; Declercq, H.; Saunders, J.; Van den Broeck, W.; Chiers, K.; Duchateau, L.; Schacht, E.; Cornelissen, M.; Gasthuys, F.; Vlaminck, L. Evaluation of an Injectable, Photopolymerizable, and Three-Dimensional Scaffold Based on Methacrylate-Endcapped Poly (D, L-Lactide-co-ε-Caprolactone) Combined with Autologous Mesenchymal Stem Cells in a Goat Tibial Unicortical Defect Model. *Tissue Eng., Part A* **2009**, *15*, 1501−1511.
(36) Van der Elst, M.; Klein, C.; de Blieck-Hogervorst, J.; Patka, P.; Haarman, H. Bone Tissue Response to Biodegradable Polymers Used for Intra Medullary Fracture Fixation: a Long-Term In Vivo Study in Sheep Femora. *Biomaterials* **1999**, *20*, 121−128.
(37) Kokubo, S.; Fujimoto, R.; Yokota, S.; Fukushima, S.; Nozaki, K.; Takahashi, K.; Miyata, K. Bone Regeneration by Recombinant Human Bone Morphogenetic Protein-2 and a Novel Biodegradable Carrier in a Rabbit Ulnar Defect Model. *Biomaterials* **2003**, *24*, 1643−1651.
(38) Mondal, T.; Sunny, M. C.; Khastgir, D.; Varma, H. K.; Ramesh, P. Poly(L-Lactide-co-ϵ-Caprolactone) Microspheres Laden with Bioactive Glass-Ceramic and Alendronate Sodium as Bone Regenerative Scaffolds. *Mater. Sci. Eng., C* **2012**, *32*, 697−706.
(39) Rohner, D.; Hutmacher, D. W.; Cheng, T. K.; Oberholzer, M.; Hammer, B. In Vivo Efficacy of Bone-Marrow-Coated Polycaprolactone Scaffolds for the Reconstruction of Orbital Defects in the Pig. *J. Biomed. Mater. Res.* **2003**, *66B*, 574−580.
(40) Abbah, S. A.; Lam, C. X.; Ramruttun, K. A.; Goh, J. C.; Wong, H.-K. Autogenous Bone Marrow Stromal Cell Sheets-Loaded mPCL/TCP Scaffolds Induced Osteogenesis in a Porcine Model of Spinal Interbody Fusion. *Tissue Eng., Part A* **2011**, *17*, 809−817.
(41) Kokubo, T.; Kushitani, H.; Sakka, S.; Kitsugi, T.; Yamamuro, T. Solutions Able to Reproduce In Vivo Surface-Structure Changes in Bioactive Glass-Ceramic A-W. *J. Biomed. Mater. Res.* **1990**, *24*, 721−734.
(42) Blaker, J. J.; Nazhat, S. N.; Maquet, V.; Boccaccini, A. R. Long-Term In Vitro Degradation of PDLLA/Bioglass Bone Scaffolds in Acellular Simulated Body Fluid. *Acta Biomater.* **2011**, *7*, 829−840.
(43) Xu, N.; Ye, X.; Wei, D.; Zhong, J.; Chen, Y.; Xu, G.; He, D. 3D Artificial Bones for Bone Repair Prepared by Computed Tomography-Guided Fused Deposition Modeling for Bone Repair. *ACS Appl. Mater. Interfaces* **2014**, *6*, 14952−14963.
(44) Yadav, D.; Agarwal, N.; Pitchumoni, C. S. A Critical Evaluation of Laboratory Tests in Acute Pancreatitis. *Am. J. Gastroenterol.* **2002**, *97*, 1309−1318.
(45) Eckardt, V.; Kanzler, G.; Rieder, H.; Ewe, K. Pancreatitis Associated with 5-Aminosalicylic Acid. *Dtsch. Med. Wochenschr.* **1991**, *116*, 540−542.
(46) Delaissé, J.-M.; Engsig, M. T.; Everts, V.; del Carmen Ovejero, M.; Ferreras, M.; Lund, L.; Vu, T. H.; Werb, Z.; Winding, B.; Lochter, A.; Karsdal, M. A.; Troen, T.; Kirkegaard, T.; Lenhard, T.; Heegaard, A.-M.; Neff, L.; Baron, R.; Foged, N. T. Proteinases in Bone Resorption: Obvious and Less Obvious Roles. *Clin. Chim. Acta* **2000**, *291*, 223−234.
(47) Ortega, N.; Behonick, D.; Stickens, D.; Werb, Z. How Proteases Regulate Bone Morphogenesis. *Ann. N. Y. Acad. Sci.* **2003**, *995*, 109−116.
(48) Gan, Z.; Yu, D.; Zhong, Z.; Liang, Q.; Jing, X. Enzymatic Degradation of Poly(ε-Caprolactone)/Poly(DL-Lactide) Blends in Phosphate Buffer Solution. *Polymer* **1999**, *40*, 2859−2862.
(49) Lu, L.; Peter, S. J.; Lyman, M. D.; Lai, H.-L.; Leite, S. M.; Tamada, J. A.; Uyama, S.; Vacanti, J. P.; Robert, L.; Mikos, A. G. In Vitro and In Vivo Degradation of Porous Poly(D, L-Lactic-co-Glycolic Acid) Foams. *Biomaterials* **2000**, *21*, 1837−1845.
(50) Galovich, L.; Perez-Higueras, A.; Altonaga, J.; Gonzalo Orden, J.; Mariñoso Barba, M.; Carrascal Morillo, M. Biomechanical, Histological and Histomorphometric Analyses of Calcium Phosphate Cement Compared to PMMA for Vertebral Augmentation in a Validated Animal Model. *Eur. Spine J.* **2011**, *20*, 376−382.
(51) Sun, G.; Zhong, J.; Liu, X.; Wei, D.; Zhou, J.; Li, W.; Jin, C.; He, D. Biodegradable Macromolecule Reticular Balloon, Manufacturing Thereof, Balloon-Sealing Apparatus and Balloon-Transporting Apparatus. Patent PCT/CN2012/001624, Dec 4, 2012.
(52) Melchels, F. P.; Bertoldi, K.; Gabbrielli, R.; Velders, A. H.; Feijen, J.; Grijpma, D. W. Mathematically Defined Tissue Engineering Scaffold Architectures Prepared by Stereolithography. *Biomaterials* **2010**, *31*, 6909−6916.
(53) Declercq, H. A.; Cornelissen, M. J.; Gorskiy, T. L.; Schacht, E. H. Osteoblast Behaviour on In Situ Photopolymerizable Three-Dimensional Scaffolds Based on D, L-Lactide, epsilon-Caprolactone and Trimethylene Carbonate. *J. Mater. Sci.: Mater. Med.* **2006**, *17*, 113−122.
(54) Nakayama, M.; Okano, T.; Miyazaki, T.; Kohori, F.; Sakai, K.; Yokoyama, M. Molecular Design of Biodegradable Polymeric Micelles for Temperature-Responsive Drug Release. *J. Controlled Release* **2006**, *115*, 46−56.
(55) Kister, G.; Cassanas, G.; Bergounhon, M.; Hoarau, D.; Vert, M. Structural Characterization and Hydrolytic Degradation of Solid Copolymers of D, L-Lactide-co-ε-Caprolactone by Raman Spectroscopy. *Polymer* **2000**, *41*, 925−932.
(56) Cho, H.; Chung, D.; Jeongho, A. Poly (D, L-Lactide-ran-ε-Caprolactone)-Poly (Ethylene Glycol)-Poly (D, L-Lactide-ran-ε-Caprolactone) as Parenteral Drug-Delivery Systems. *Biomaterials* **2004**, *25*, 3733−3742.
(57) Calandrelli, L.; Calarco, A.; Laurienzo, P.; Malinconico, M.; Petillo, O.; Peluso, G. Compatibilized Polymer Blends Based on PDLLA and PCL for Application in Bioartificial Liver. *Biomacromolecules* **2008**, *9*, 1527−1534.
(58) Zhang, Z.; Rouabhia, M.; Wang, Z.; Roberge, C.; Shi, G.; Roche, P.; Li, J.; Dao, L. H. Electrically Conductive Biodegradable Polymer Composite for Nerve Regeneration: Electricity-Stimulated Neurite Outgrowth and Axon Regeneration. *Artif. Organs* **2007**, *31*, 13−22.
(59) Uto, K.; Muroya, T.; Okamoto, M.; Tanaka, H.; Murase, T.; Ebara, M.; Aoyagi, T. Design of Super-Elastic Biodegradable Scaffolds with Longitudinally Oriented Microchannels and Optimization of the Channel Size for Schwann Cell Migration. *Sci. Technol. Adv. Mater.* **2012**, *13*, 064207.
(60) Meretoja, V.; Helminen, A.; Korventausta, J.; Haapa-aho, V.; Seppälä, J.; Närhi, T. Crosslinked Poly(ϵ-Caprolactone/D,L-Lactide)/Bioactive Glass Composite Scaffolds for Bone Tissue Engineering. *J. Biomed. Mater. Res., Part A* **2006**, *77A*, 261−268.
(61) Meretoja, V. V.; Tirri, T.; Malin, M.; Seppälä, J. V.; Närhi, T. O. Ectopic Bone Formation in and Soft-Tissue Response to P (CL/DLLA)/Bioactive Glass Composite Scaffolds. *Clin. Oral Implan. Res.* **2014**, *25*, 159−164.

DOI: 10.1021/acsami.5b04868
ACS Appl. Mater. Interfaces 2015, 7, 18540−18552